Molecular Therapy
Nucleic Acids
Original Article

Direct Delivery of Apatite Nanoparticle-Encapsulated siRNA Targeting TIMP-1 for Intractable Abnormal Scars

Masayo Aoki,[1,2] Noriko M. Matsumoto,[1] Teruyuki Dohi,[1] Hiroaki Kuwahawa,[3] Satoshi Akaishi,[3] Yuri Okubo,[1] Rei Ogawa,[1] Hirofumi Yamamoto,[4] and Kazuaki Takabe[5,6]

[1]Department of Plastic, Reconstructive, and Aesthetic Surgery, Nippon Medical School, Tokyo 113-8603, Japan; [2]Department of Biochemistry and Molecular Biology, Nippon Medical School, Tokyo, Japan; [3]Department of Plastic and Reconstructive Surgery, Nippon Medical School Musashi Kosugi Hospital, Kanagawa, Japan; [4]Department of Molecular Pathology, Osaka University, Osaka, Japan; [5]Division of Breast Surgery, Department of Surgical Oncology, Roswell Park Comprehensive Cancer Center, Buffalo, NY, USA; [6]Department of Surgery, University at Buffalo Jacob School of Medicine and Biomedical Sciences, The State University of New York, Buffalo, NY, USA

Hypertrophic scars (HSs) and keloids are histologically characterized by excessive extracellular matrix (ECM) deposition. ECM deposition depends on the balance between matrix metalloproteinases (MMPs) and tissue inhibitors of metalloproteases (TIMPs). TIMP-1 has been linked to ECM degradation and is therefore a promising therapeutic strategy. In this study, we generated super carbonate apatite (sCA) nanoparticle-encapsulated TIMP-1 small interfering RNA (siRNA) (siTIMP1) preparations and examined the effect of local injections on mouse HSs and on *ex vivo*-cultured keloids. The sCA-siTIMP1 injections significantly reduced scar formation, scar cross-sectional areas, collagen densities, and collagen types I and III levels in the lesions. None of the mice died or exhibited abnormal endpoints. Apatite accumulation was not detected in the other organs. In an *ex vivo* keloid tissue culture system, sCA-siTIMP1 injections reduced the thickness and complexity of collagen bundles. Our results showed that topical sCA-siTIMP1 injections during mechanical stress-induced HS development reduced scar size. When keloids were injected three times with sCA-siTIMP1 during 6 days, keloidal collagen levels decreased substantially. Accordingly, sCA-siRNA delivery may be an effective approach for keloid treatment, and further investigations are needed to enable its practical use.

INTRODUCTION

Hypertrophic scars (HSs) and keloids are abnormally growing scars that are histologically characterized by chronic inflammation and excessive extracellular matrix (ECM) deposition.[1] Keloids are elastic nodular lesions that contain thick and complex keloidal collagens.[2,3] Although HSs and keloids have several histologically distinct characteristics, it is sometimes difficult to distinguish between them.[4] Clinically, keloids have characteristic shapes, including dumbbells and butterflies. Based on the shapes and direction of extension, local mechanical forces are an important risk factor for the development and progression of these abnormal scars.[5] Genetic factors, including single-nucleotide polymorphisms, are also risk factors for keloids.[6] These intractable abnormal scars are unique to humans, and the mechanisms underlying their development are still unclear.[7]

Although many treatment approaches have been used for keloids, their overall effect sizes are small and, consequently, long treatment periods are required.[8] Steroids, a conservative treatment approach, generally take several years to treat even single, small lesions.[9] Surgical resection followed by radiation therapy is conventionally applied in severe cases.[10] However, the risk of recurrence is high and additional long-term treatments are essential.[11] Laser therapy, botulinum toxin A, and fluorouracil are common additional therapies.[12,13] The lack of a treatment that resolves inflammation or reduces keloids with satisfactory efficiency limits the quality of life of patients.

A more efficient treatment approach would be to effectively degrade excess ECM. The degradation or deposition of ECM depends on the balance between matrix metalloproteinases (MMPs) and tissue inhibitors of metalloproteases (TIMPs), which belong to a family of structurally related enzymes. While MMPs degrade the ECM, TIMPs inhibit MMPs, thereby favoring ECM deposition.[14] The mRNA expression levels of *TIMP1* and *TIMP2* are significantly higher in abnormal scar tissues than in normal scars, and the expression of *TIMP1* is significantly higher in keloid tissues than in HSs.[15] We previously reported that when keloid-derived fibroblasts are transduced via a lentiviral vector with small interfering RNA (siRNA) targeting TIMP-1, the ECM produced by the fibroblasts exhibits net degradation; siRNA targeting TIMP-2 did not have this effect.[16,17] Thus, TIMP-1 knockdown may effectively promote ECM degradation in keloids. This novel anti-fibrotic treatment has potential therapeutic applications for keloids.

Received 20 April 2020; accepted 7 August 2020;
https://doi.org/10.1016/j.omtn.2020.08.005.

Correspondence: Masayo Aoki, Department of Plastic, Reconstructive, and Aesthetic Surgery, Nippon Medical School, 1-1-5 Sendagi, Bunkyo, Tokyo 113-8603, Japan.
E-mail: masayok@nms.ac.jp

A

siRNA sequences	
siControl	5'-AUCCGCGCGAUAGUACGUAUUdTdT-3'
siTIMP1-A	5'-ACUGCAGAGUGGCACUCAUUGdTdT-3'
siTIMP1-B	5'-ACAGACGGCCUUCUGCAAUUCdTdT-3'
siTIMP1-C	5'-GCACAGUGUUUCCCUGUUUAUdTdT-3'

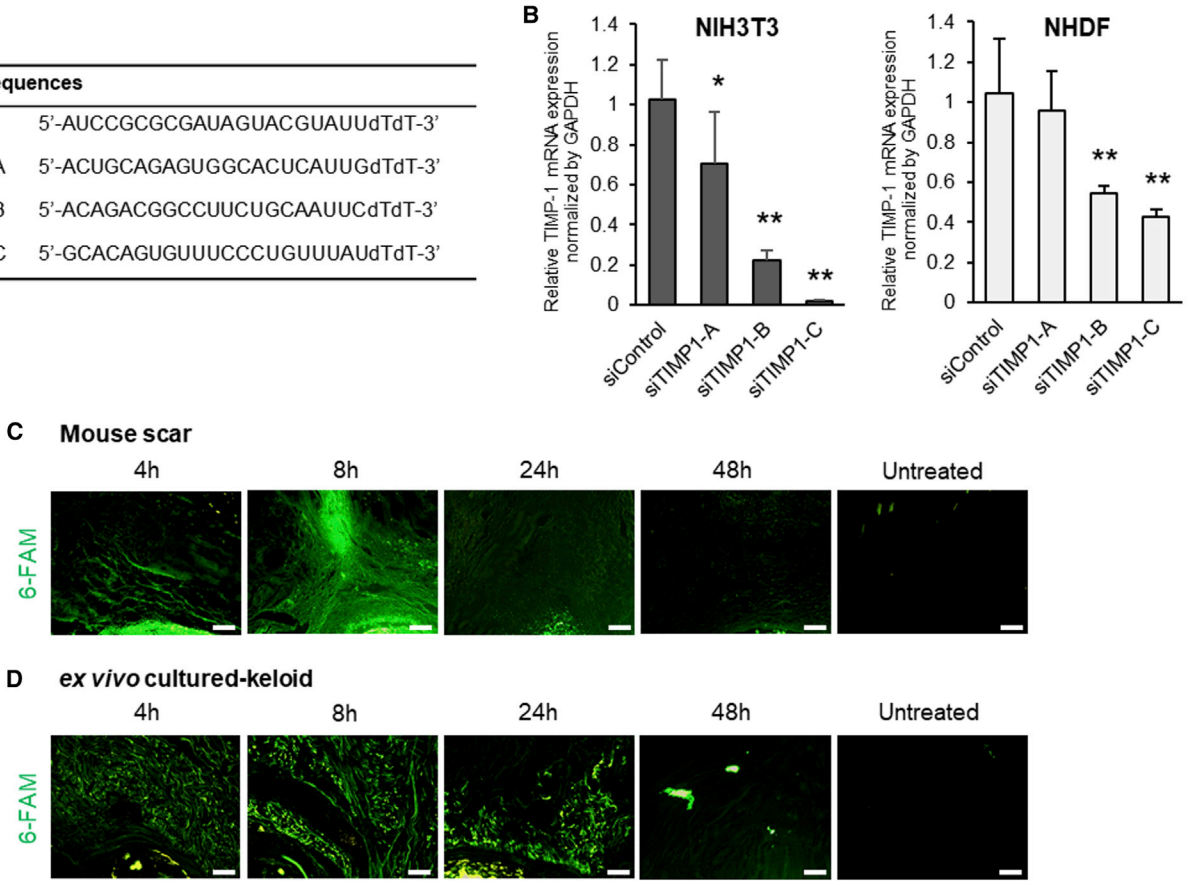

Figure 1. siRNA Design, Knockdown Efficiency *In Vitro*, and Clearance of sCA-siRNA after Injection into Murine HSs and Cultured Keloids

(A) siRNA sequences used in this study. (B) qRT-PCR analysis of *TIMP1* mRNA levels in NIH 3T3 cells and NHDFs 18 h after transfection with three transduction units per cell of three sCA-siRNAs targeting TIMP-1 (siTIMP1) (A–C) or a control sequence (siCON). All values were normalized to the level of *GAPDH* (n = 6 wells per treatment per cell type). (C and D) Murine HSs (C) and cultured keloids (representative of four mice) (D) were injected with 6-FAM-labeled sCA-siCON and subjected to fluorescence imaging 4, 8, 24, and 48 h later (scale bars, 100 μm). The values shown are means ± SD. *$p < 0.05$, **$p < 0.01$, as determined by the Tukey-Kramer method after one-way factorial ANOVA.

However, siRNA-expressing viral vector delivery has issues related to safety, side effects, and immunogenicity. One strategy to improve clinical applications may be to encapsulate siRNAs with nanoparticles of apatite, a constituent of vertebrate tissues. The direct, transient, and safe delivery of siRNA would be an easy approach with highly specific effects. To test the clinical applicability of TIMP-1 siRNA treatment for keloids, we generated super carbonate apatite (sCA)-encapsulated TIMP-1 siRNA preparations, as previously reported.[18] These nanoparticles accumulate in fibrotic tumor lesions due to increased permeability and retention associated with vascular endothelial cell misalignment and lymphatic drainage disorders.[19] We examined the effect of local injections of these preparations on mouse HS growth and on keloidal collagen in *ex vivo*-cultured human keloids.

RESULTS

siTIMP1 Sequences and Their Knockdown Efficiency *In Vitro*

First, we designed three siRNA sequences targeting both human and mouse TIMP-1 (siTIMP1-A–C) (Figure 1A) and encapsulated them with sCA, as described previously.[18] We used these preparations for the *in vitro* transfection of mouse dermal fibroblasts (NIH 3T3) and normal human dermal fibroblasts (NHDFs).[20] Of the three siRNAs, siTIMP1-C knocked down *TIMP1* mRNA expression most effectively in both lines (Figure 1B).

Clearance of sCA-Encapsulated siRNA after Injection into Murine HSs and Cultured Resected Keloids

We generated mechanical stress-induced HSs in mice as described previously[21,22] and cultured seven keloids *ex vivo* after resection from seven patients.[23] To examine the rate of sCA-encapsulated siRNA clearance from these tissues after injection, we labeled the sCA-encapsulated control siRNA (sCA-siCON) with 6-carboxyfluorescein-aminohexyl phosphoramidite (6-FAM).[24] In both tissues, strong fluorescence was detected 8 h after a single injection; 48 h later, fluorescence was significantly attenuated (Figures 1C and 1D). Notably, the specific accumulation of sCA-siCON in the scar area was observed 8 h post-injection in mouse HSs (Figure 1C). Thus, the sCA-encapsulated siRNAs were cleared within 48 h.

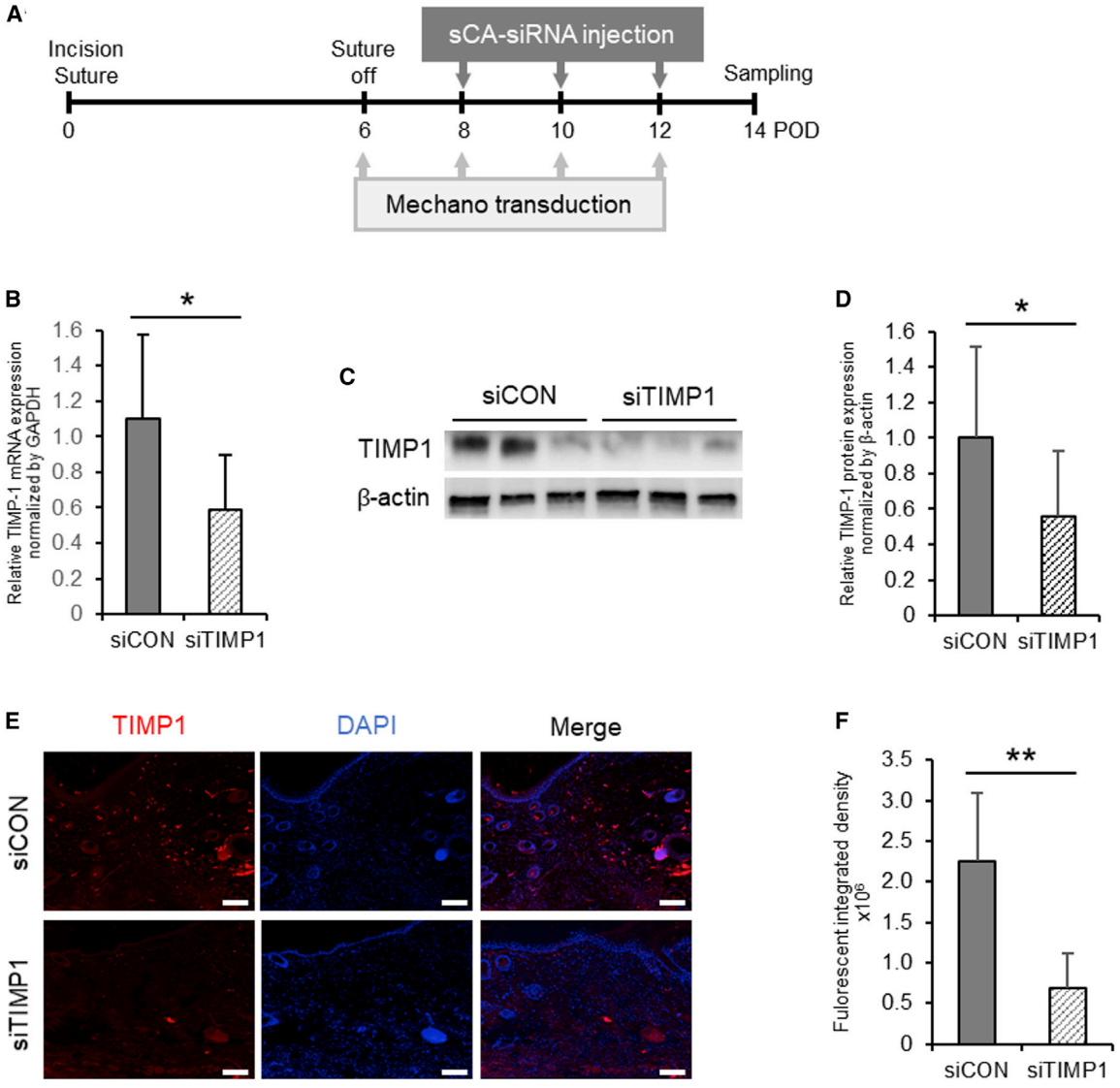

Figure 2. Effectiveness of sCA-siRNA-Mediated TIMP-1 Knockdown in Murine HSs

(A) Schematic depiction of the schedule for the generation of mechanical force-induced HSs in mice and injection with sCA-siTIMP1 or siCON. This experiment was repeated independently five times with three to four mice per treatment, and the RNA and protein levels estimated in two and four of these experiments were used for the analyses, respectively. (B) qRT-PCR analysis of *TIMP1* mRNA levels in the siCON- and siTIMP1-injected HSs on day 14. All values were normalized to the level of *GAPDH* (n = 12 mice per treatment). (C) Western blot showing TIMP-1 protein expression in the siCON- and siTIMP1-injected HSs on day 14. (D) Quantitation of the day 14 western blot data. All values were normalized to the level of β-actin (n = 12 mice per treatment). **$p < 0.01$, as determined by a Wilcoxon signed-rank test. (E) Representative images after fluorescence immunoassay of TIMP-1 expression in the siCON- and siTIMP1-treated HSs on day 14 (scale bars, 100 μm). (F) Quantitation of the integrated fluorescent density on day 14 (n = 9 mice per treatment). *$p < 0.05$, as determined by a Student's t test or Welch's t test after F tests. All values are means ± SD.

Efficacy of sCA-siTIMP1 in Mouse HSs

We then intradermally injected the mechanical stress-induced murine HSs three times with sCA-siCON or TIMP1-C siRNA (designated sCA-siTIMP1) according to the schedule shown in Figure 2A. On day 14, quantitative RT-PCR (qRT-PCR) and immunoblotting showed that the sCA-siTIMP1 injections significantly reduced TIMP-1 at the mRNA ($p = 0.011$) (Figure 2B) and protein levels ($p = 0.023$) in the scars (Figures 2C and 2D). A TIMP-1 immunofluorescence analysis also showed the significant attenuation of TIMP-1-related fluorescence in scars injected with sCA-siTIMP, but not in scars injected with sCA-siCON ($p < 0.001$) (Figures 2E and 2F).

sCA-siTIMP1 Injection Is Associated with Reduced HS Formation in Mice

When murine HSs were injected with sCA-siTIMP1, they displayed noticeably smaller scar areas on day 14 than did those of the HSs

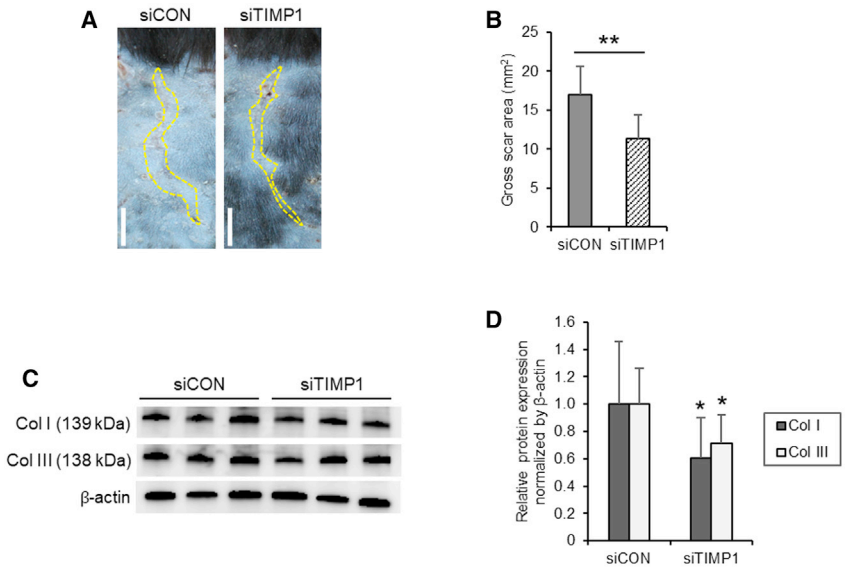

Figure 3. Effect of Injections of sCA-siRNA against TIMP-1 on Murine HS Growth and Collagen Expression

(A) Representative images of the gross scar area (dotted lines) of the sCA-siTIMP1- and sCA-siCON-injected HSs on day 14 (scale bars, 5 mm). (B) Quantitation of the gross scar area on day 14 (n = 16 mice per treatment). (C) Western blot images showing collagen type I (Col I) and III (Col III) protein expression in the siCON- and siTIMP1-injected HSs on day 14. (D) Quantitation of the day 14 western blot data. All values were normalized to the level of β-actin (n = 12 mice per treatment). All values are means ± SD. *$p < 0.05$, **$p < 0.01$, as determined by a Student's t test or Welch's t test after F tests.

injected with sCA-siCON (Figure 3A). These differences were significant when the gross scar area on day 14 was quantified ($p < 0.001$) (Figure 3B). Moreover, an immunoblot analysis of the same scars showed that, compared with the sCA-siCON injections, the sCA-siTIMP1 injections significantly reduced the protein levels of collagen types I ($p = 0.030$) and III ($p = 0.012$) in the HS lesions (Figures 3C and 3D).

These observations were consistent with our finding that, compared with sCA-siCON-treated mice,[25] sCA-siTIMP1-treated mice have noticeably smaller cross-sectional scar areas on day 14, as evaluated by Masson's trichrome staining and picrosirius red staining under polarized light (Figure 4A). Our quantitative analysis of the cross-sectional scar area and estimates of the scar elevation index in Masson's trichrome-stained sections confirmed that sCA-siTIMP1 significantly suppressed scarring ($p = 0.019$ and 0.032, respectively) (Figures 4B and 4C).

The sCA-siTIMP1-treated mice also had noticeably smaller collagen densities on day 14, as shown by high magnification images of the Masson's trichrome-stained sections and polarization (Figure 4D). Our quantitative analyses of the collagen area and polarized integrated density in the picrosirius red-stained sections under polarized light confirmed that the sCA-siTIMP1 injections significantly reduced the collagen density in scars ($p = 0.018$ and 0.045, respectively) (Figures 4E and 4F).

Efficacy of sCA-siTIMP1 in *Ex Vivo*-Cultured Keloid Tissues

We then subjected the cultured resected keloids from seven patients to three injections with sCA-siCON or sCA-siTIMP1 according to the schedule shown in Figure 5A.[26] The characteristics of the patients are summarized in Figure 5B. qPCR and immunoblot analyses on day 6 showed that the sCA-siTIMP1 injections significantly reduced TIMP-1 expression at the mRNA ($p < 0.001$) and protein levels ($p = 0.002$) in keloids (Figures 5C–5E). PCR was performed using four keloids and was repeated on three to four pieces per keloid. The immunoblot experiment was performed using four keloids and was repeated three or more times per keloid. Similarly, an immunofluorescence analysis of eight pieces each from three keloids showed that sCA-siTIMP1, but not sCA-siCON, significantly attenuated TIMP-1-related fluorescence in keloid tissues ($p < 0.001$) (Figures 5F and 5G).

sCA-siTIMP1 Injection Reduces Keloidal Collagen in *Ex Vivo*-Cultured Keloids

The preoperative findings and pathological analysis of a shoulder and an ear keloid from patients K4 and K5 immediately after resection and after 6 days of *ex vivo* culture with sCA-siRNA injections are shown in Figures 6A and 6B, respectively. The thickness and complexity of the collagen bundles (i.e., keloidal collagen) were noticeably lower after sCA-siTIMP1 injections than after sCA-siCON injections.[4,27] Similar histological effects were confirmed for a pubic keloid from patient K7.

An immunoblot analysis of cultured keloids showed that, compared with the sCA-siCON injections, the sCA-siTIMP1 injections significantly reduced the protein levels of collagen types I ($p = 0.014$) and III ($p = 0.046$) (Figures 7A and 7B). This is consistent with the results of our histological analysis of three keloids after injections with sCA-siTIMP1 or sCA-siCON. Polarization microscopy also showed that sCA-siTIMP1 injections clearly reduced the collagen density in keloids (Figure 7C). Quantification of the polarized integrated density from low-magnification images showed that the sCA-siTIMP1 injections significantly decreased the collagen density ($p < 0.001$) (Figure 7D).

Off-Target Effects of sCA-siTIMP1 *In Vitro* and *In Vivo* Toxicity after HS Injections

The transfection of NIH 3T3 cells with sCA-siTIMP1 resulted in changes in the expression levels of 111 genes, including in several non-coding RNA genes (Figure 8A). In total, 97 genes were downregulated by ≥2-fold and 14 were upregulated by >2-fold (Table S1).[28] We next investigated whether siRNA delivery by sCA has side effects *in vivo*. In particular, we examined the effect of sCA-siRNA injections

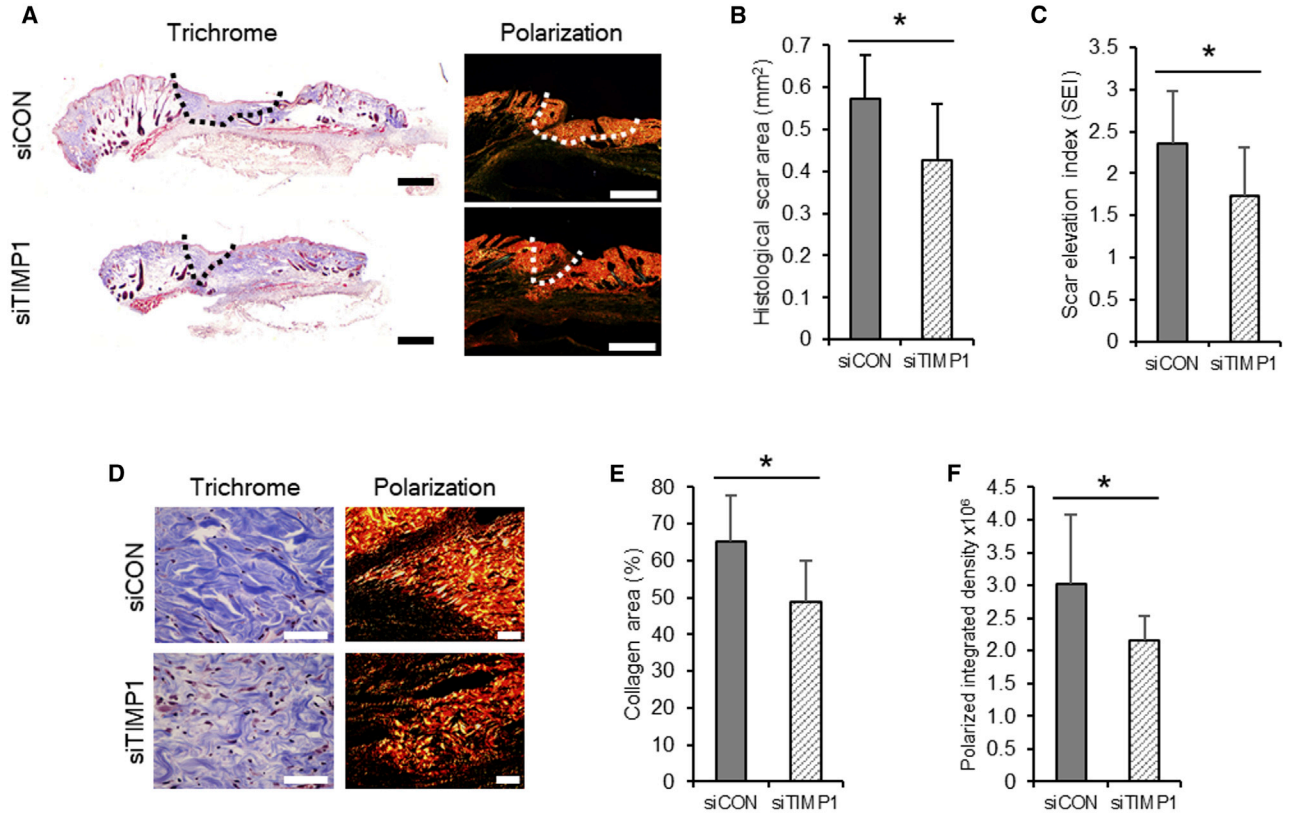

Figure 4. Histological Effect of the Injection of sCA-siRNA against TIMP-1 on Murine HS Growth and Collagen Density

(A) Representative images of the Masson's trichrome-stained cross-sectional scar area (dotted line) (scale bar: 500 μm) of the siCON- and siTIMP1-injected HSs on day 14. Polarization images of the same samples are also shown (scale bars, 500 μm). (B) Quantitation of the cross-sectional scar area on day 14 (n = 9 mice per treatment). (C) Cross-sectional scar elevation index (SEI) of the siCON- and siTIMP1-injected HSs on day 14 (n = 9 mice per treatment). SEI is defined as the scar thickness divided by the thickness of the adjacent normal skin. (D) Representative images of the Masson's trichrome-stained collagen density in the siCON- and siTIMP1-injected HSs on day 14 (scale bars, 50 μm). Polarization images of the same samples are also shown (scale bars, 50 μm). (E) Quantitation of the percentage of scar area that was occupied by collagen on day 14 (n = 9 mice per treatment). (F) Quantitation of the polarized integrated density on day 14 (n = 9 mice per treatment). All values are means ± SD. *$p < 0.05$, as determined by a Student's t test or Welch's t test after F tests.

in murine HS lesions on blood electrolyte levels. sCA is a biological component of calcium-containing vertebrates, and we also investigated whether the injections result in calcium accumulation in organs. During the experiment, none of the mice died. In addition, none of the mice exhibited abnormal blood electrolyte levels on day 14 (Figure 8B). Moreover, apatite accumulation was not detected in the livers, kidneys, hearts, lungs, or intestines on day 14 (Figure 8C). These findings are consistent with those of Wu et al.,[18] who evaluated the systemic delivery of sCA-siRNA.

DISCUSSION

Severe keloids that respond poorly to current treatments require potent and highly specific ECM degradation. Our study showed that topical sCA-siTIMP1 injections during mechanical stress-induced HS development significantly reduce collagen accumulation and scar size. Interestingly, when human keloids were injected three times with sCA-siTIMP1 during 6 days, keloidal collagens disappeared, suggesting that this approach might be useful for the treatment of keloids. This is supported by recent studies showing that siRNA delivery is effective for several skin diseases, including skin cancers, psoriasis, vitiligo, dermatitis, and leprosy.[29]

The clinical application of siRNA-mediated mRNA knockdown has been a focus of research in the past decade owing to the high specificity with which it suppresses target molecules.[30] The local delivery of siRNAs, particularly in dermatological applications, effectively knocks down targets.[31] As a result, considerable research has examined the effectiveness and safety of various non-viral drug delivery systems (DDSs).[32] Nanoparticle-mediated siRNA delivery has key advantages, including specificity, potency, and duration of effects.[33,34] An efficient method for nanoparticle delivery is direct injection. Different types of nanoparticles have been developed to regulate ocular wound healing.[35] For topical treatment of skin diseases such as diabetic wounds, psoriasis, inflammatory diseases, and fibrosis, lipid nanoparticles,[36] a cationic star-shaped polymer,[37] spherical nucleic acid-gold nanoparticle conjugates,[38] and mesoporous silica-based nanoparticles[39] have been developed.

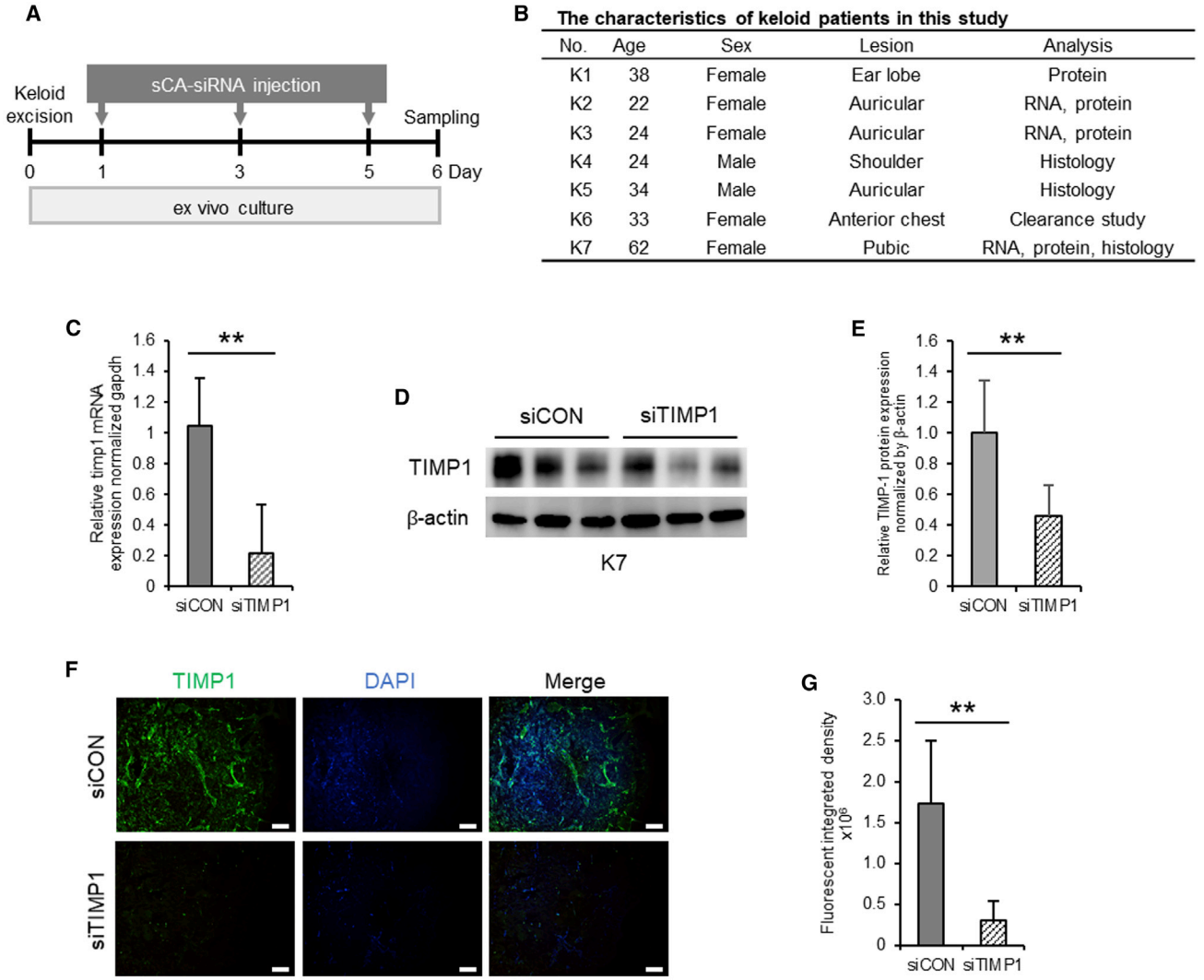

Figure 5. Ability of sCA-siRNA against TIMP-1 to Knock Down TIMP-1 Levels in *Ex Vivo*-Cultured Keloid Tissues

(A) Schematic depiction of the schedule for the injection of *ex vivo*-cultured keloid tissues with sCA-siTIMP1 or sCA-siCON. (B) Characteristics of patients with keloids included in this study. (C) qRT-PCR analysis of *TIMP1* mRNA levels in the siCON- and siTIMP1-injected keloid tissues on day 6. All values were normalized to the level of *GAPDH* (n = 10 keloid pieces from three patients per treatment). (D) Western blot image showing TIMP-1 protein expression in the siCON- and siTIMP1-injected scars on day 6. (E) Quantitation of the day 14 western blot data. All values were normalized to the level of β-actin (n = 9 keloid pieces from four patients per treatment). (F) Fluorescent TIMP-1-immunostained images of the siCON- and siTIMP1-injected keloid tissues on day 6 (scale bars, 200 μm). (G) Quantitation of the fluorescent integrated density in day 6 (n = 10 keloid pieces from three patients per treatment). All values are means ± SD. *$p < 0.05$, **$p < 0.01$, as determined by a Student's t test or Welch's t test after F tests.

In the present study, we delivered the target molecule (TIMP-1 siRNA) by encapsulation with apatite nanoparticles and injection into scars. In 2007, Chowdhury et al.[20] showed that carbon apatite is an excellent DNA carrier for efficient transfection into mammalian cells *in vitro*. Wu et al.[18] then reduced the size of the carbonate apatite particles to the nano level by sonication to create sCA. The sCA particles are very small (10–20 nm) and readily penetrate solid lesions *in vivo*. Our group recently showed that topically applied sCA effectively transfects the wound bed in mice.[40] Wu et al.[18] also reported that if relatively large particles that contaminate sCA can be removed, the resulting purified sCA preparation is very safe in mice and monkeys. In addition, sCA preparation does not require special reagents or equipment and involves only simple methods. These findings together suggest that sCA is a suitable DDS for the delivery of siRNA as well as other molecules into solid lesions.[19] Our study of mice showed that sCA accumulates specifically in scar tissues. As sCA accumulates due to increased permeability and retention associated with blood and lymph flow, it is expected to accumulate in chronic inflammatory lesions, such as abnormal scars. Keloids are particularly suited to a small particle carrier-based DDSs, such as sCA, because

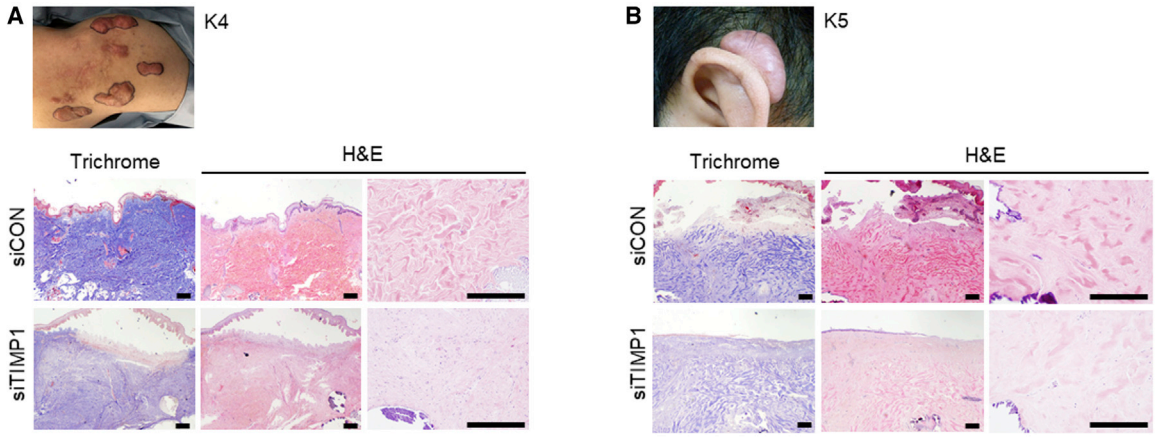

Figure 6. Effect of Injection with sCA-siTIMP1 on Keloidal Collagen in *Ex Vivo*-Cultured Keloid Tissues

(A and B) Keloids were resected from K4 (a 24-year-old male with a shoulder keloid) (A) and K5 (a 34-year-old male with an auricular keloid) (B). Preoperative findings are shown. The keloids were subjected to *ex vivo* culture and injected with sCA-siCON or sCA-siTIMP1. Representative images of the keloid tissues on day 6 after Masson's trichrome and H&E staining are shown (scale bars, 300 μm).

they are hard fibrotic and inflammatory masses in the skin that do not permit the ready diffusion of larger molecules after injection. The safety of sCA also makes it particularly suitable for keloids, which are not lethal.

Note, however, that siRNA therapy may have unwanted off-target effects on other RNAs or proteins. Indeed, we identified 111 genes whose expression in murine fibroblasts may have been altered by TIMP-1 knockdown, including several non-coding RNAs. Since intermolecular interactions with non-coding RNAs play a central role in gene regulation,[41] it will be essential to clarify the precise effects of the TIMP-1 siRNA-associated gene fluctuations. Moreover, because the functions of many non-coding RNAs are still unknown,[42] further functional assays and the development of a system to predict side effects due to off-target effects are needed.[43]

The mechanisms underlying keloid formation and growth remain unclear. However, a key pathological factor is chronic inflammation and the induction of cytokine and chemokine production, which in turn provokes marked angiogenesis and fibrosis.[44] As a result, conservative treatments for the local symptoms of keloids should target one or more of these features.[45] Indeed, the main conservative treatment at present is corticosteroids, which suppress chronic inflammation in keloids. However, this approach requires long-term treatment and close follow-up. Consequently, there is an ongoing and profound need for more effective therapeutic agents. A recently developed alternative is FTY720, which suppresses both chronic inflammation and angiogenesis.[46] Another option may be botulinum toxin A, although the mechanism by which it ameliorates keloid growth and symptoms remains unclear.[13] These new drugs may be particularly useful for patients whose keloids respond poorly to steroids. New drugs are also needed for severe keloids because although surgery followed by irradiation has excellent outcomes,[47] the resection site must be monitored very closely via a long-term postoperative management program. Indeed, some patients must continue treatment for their entire lives. Thus, effective conservative therapies for all types of keloids are needed. Our study suggests that injections of sCA-encapsulated siRNAs against TIMP-1 may be an effective option. This finding is supported by a recent study by Castleberry et al., who showed that the administration of silk sutures coated with a nano layer of a polymer containing an siRNA targeting connective tissue growth factor to third-degree burns in rats improves tissue remodeling and reduces contraction.[48]

In terms of mechanisms of action, the observation that TIMP-1 siRNA not only eliminated keloidal collagen in existing keloids, but it also impaired mechanical stress-induced collagen accumulation, and HS growth suggests that unlike corticosteroids, it primarily acts as an anti-fibrotic agent. Mechanical stress on the wound/scar is a well-known risk factor for keloid formation and progression.[5] It is thought that this stress acts by initiating and/or promoting the chronic inflammation that drives pathological collagen accumulation and scar development. The stiff fibrosis that results from inflammation then exacerbates the influence of mechanical stress at the histological level, which in turn amplifies inflammation in the scar.[49] Thus, our TIMP-1 siRNA may be a viable anti-fibrotic treatment approach for keloids, particularly when combined with treatments that target inflammation and/or capillary growth. However, further investigations of this approach, including analyses of off-target effects and side effects, are required before it can be put into practical use.

MATERIALS AND METHODS

Cells

Murine dermal fibroblast NIH 3T3 cells were purchased from ATCC (Manassas, VA, USA) and cultured in Dulbecco's modified Eagle's medium (DMEM) containing 10% fetal bovine serum (FBS). NHDFs were purchased from TaKaRa (Kusatsu, Japan) and cultured in

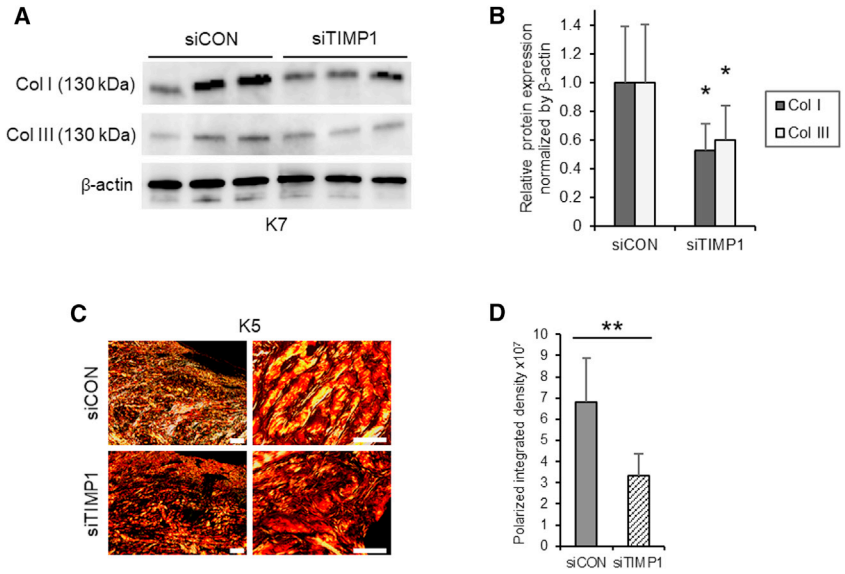

Figure 7. Effect of Injection with sCA-siTIMP1 on Collagen Expression and Density in *Ex Vivo*-Cultured Keloid Tissues

(A) Western blot images showing Col I and Col III protein expression in the siCON- and siTIMP1-injected keloid tissues on day 6. (B) Quantitation of the day 14 western blot data. All values were normalized to the level of β-actin (n = 8 keloid pieces from four patients per treatment). (C) Representative images of polarization microscopy of the same keloid tissues are also shown (scale bars, left, 200 μm; right, 50 μm). (D) Quantitation of the polarized integrated density on day 6 (n = 10 keloid pieces from the three patients per treatment). All values are means ± SD. *$p < 0.05$, **$p < 0.01$ as determined by a Student's t test or Welch's t test after F tests.

fibroblast growth medium 2 supplement mix (TaKaRa) supplemented with 10% FBS. Recombinant human transforming growth factor β1 (TGF-β1) was purchased from R&D Systems (Minneapolis, MN, USA).

Mice

All animal procedures were approved by the Animal Experimental Ethics Review Committee of Nippon Medical School (28-063) and were performed according to the institutional guidelines for animal care (Nippon Medical School, Tokyo, Japan). Eight-week-old male C57BL6/N mice were purchased from Tokyo Experimental Animals Supply (Tokyo, Japan).

siRNA

Control siRNA and TIMP-1 siRNAs for both *in vitro* and *in vivo* use were purchased from Aji Biopharma (Osaka, Japan). 6-Carboxyfluorescein-labeled control siRNA was purchased from Aji Biopharma and was used for *in vivo* and *ex vivo* fluorescence microscopy experiments.

Preparation of sCA Nanoparticle-Encapsulated siRNAs

For *in vitro* use, sCA-siRNAs were prepared as described previously.[18] Briefly, 4 μL of 1 M $CaCl_2$ was incubated at 37°C for 30 min with 2 μg of siRNA in 1 mL of an inorganic solution (44 mM $NaHCO_3$, 0.9 mM NaH_2PO_4, 1.8 mM $CaCl_2$ [pH 7.5]) and then centrifuged at 12,000 rpm for 3 min. After the pellet was dissolved in culture medium, the solution was sonicated in a water bath for 10 min to generate sCA-siRNA. For *in vivo* use, sCA-siRNAs were prepared in the same way at a 25-fold scale. Briefly, 100 μL of 1 M $CaCl_2$ was incubated at 37°C for 30 min with 50 μg of siRNA in 25 mL of an inorganic solution and then centrifuged. The pellet was dissolved in 100 μL of saline containing 0.5% mouse serum albumin and then sonicated.

In Vitro Transfection

To confirm the *in vitro* transfection efficiency of sCA-siRNAs in fibroblasts, 2×10^5 cells were cultured in six-well plates for 24 h and then incubated with the sCA-siRNA-medium solution for 18 h. After comparing the data from several conditions, the transfection efficiency was evaluated in the presence of 10 ng/mL TGF-β1. The cells were collected for total RNA isolation.

Mechanical Load-Induced Mouse HS Model and sCA-siRNA Injection

Model HSs were generated by biomechanical loading induced by Vector 620 expansion screws (Scheu, Iserlohn, Germany) as previously described.[21] Briefly, a 2-cm-long full-thickness incision created on the dorsal midline of each mouse was sutured with 4-0 Vicryl (Johnson & Johnson, New Brunswick, NJ, USA). The sutures were removed on day 6 after incision. The mechanical loading device was placed above the scars and then sutured to the skin on either side of the incision with 5-0 Ethilon (Johnson & Johnson). Sustainable stretching was performed on days 6, 8, 10, and 12. sCA was mixed with 50 μg of siRNA and pelleted. The pellet was then dissolved in 100 μL of saline containing 0.5% mouse serum albumin. Given that the *ex vivo* half-life of sCA-siRNAs cultured with mouse serum is approximately 30 h,[18] and that the effect of mechanical loading on HS formation in mice is remarkable after day 14,[22] the 2-cm-long HS on each mouse was injected every other day (on days 8, 10, and 12 after stretching) with 100 μL of sCA-siCON or sCA-siTIMP1. The samples were harvested 14 days after incision for RNA and protein isolation and histological analysis.

Ex Vivo Culture of Keloid Tissues

Ex vivo culture of keloid tissues was performed as described previously.[23] Briefly, the keloid tissue was cut into 10 × 10 × 10-mm sections and incubated in DMEM containing 10% FBS and 1% antibiotic-antimycotic (Thermo Fisher Scientific, Waltham, MA, USA) for 24 h. The tissues were injected every other day with 100 μL of sCA-siCON or sCA-siTIMP1. The specimens were incubated for 6 days. Keloid tissues were then used for RNA and protein isolation or were fixed in 4% paraformaldehyde and subjected to H&E staining

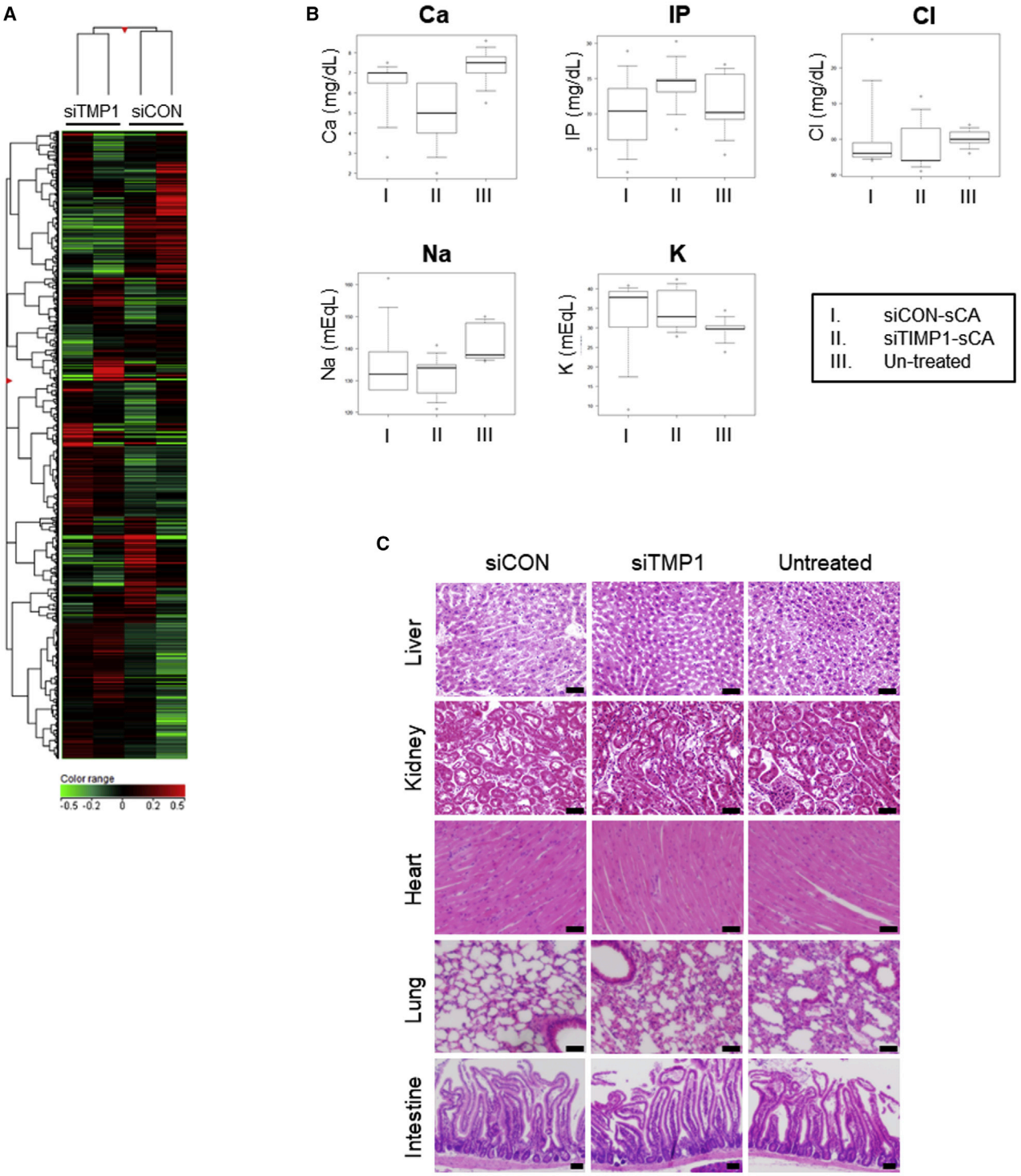

Figure 8. *In Vitro* Gene Expression, Blood Electrolyte Levels, and Histopathology of the Other Organs in Mice with sCA-siRNA-Injected HSs

(A) Heatmap of gene expression profiling in NIH 3T3 cells 18 h after transfection with sCA-encapsulated siRNAs that targeted TIMP-1 (siTIMP1) or a non-targeting siRNA (siCON) (n = 2). (B) The murine HSs were injected with sCA-encapsulated siRNAs as shown in Figure 2A and the effects of the treatment on blood electrolyte levels on day 14 were determined. The electrolytes that were examined were calcium (Ca), inorganic phosphorus (IP), chlorine (Cl), sodium (Na), and potassium (K). (C) The livers, kidneys, hearts, lungs, or intestines of the mice on day 14 were subjected to histology and H&E staining. Representative images are shown (scale bars, 50 μm). All values are means ± SD (n = 8 mice per treatment). The control and TIMP-1 siRNAs did not differ significantly in terms of any of these variables, as determined by the Tukey-Kramer method after one-way factorial ANOVA.

following standard protocols. This study was approved by the Ethics Committee at Nippon Medical School, Tokyo, Japan (30-11-1039).

sCA-siRNA Clearance Study

The 2-cm-long scars on HS-model mice were injected once with 100 μL of sCA-6-carboxyfluorescein-labeled control siRNA on day 9 after wounding. The *ex vivo* cultured keloid tissues were also injected once with the same solution. The samples were harvested 4, 8, 24, and 48 h after the injection for imaging. Frozen 25-μm-thick sections were then evaluated using a fluorescence microscope (Olympus, Tokyo, Japan).

qRT-PCR

Total RNA was extracted by using TRIzol regent (Invitrogen, Carlsbad, CA, USA) and an RNeasy mini kit (QIAGEN, Hilden, Germany) according the manufacturer's recommendations. The quantity of RNA was determined by spectrophotometry using an ND-2000 NanoDrop (Thermo Fisher Scientific). cDNA was synthesized using a high-capacity cDNA reverse transcription kit (Applied Biosystems, Foster City, CA, USA). qRT-PCR was performed by using an ABI Prism 7500 system (Applied Biosystems) with Power SYBR Green master mix (Applied Biosystems). For each primer set, the optimal dilution was determined and melting curves were used to determine the amplification specificity. *GAPDH* served as the internal control. The primer pairs used were as follows: mouse *TIMP1*, forward, 5′-CGGACCTGGTCATAAGGGCTA-3′, and reverse, 5′-GGGCA TATCCACAGAGGCTT-3′; mouse *GAPDH*, forward, 5′-AGGTC GGTGTGAACGGATTTG-3′, and reverse, 5′-TGTAGACCATGTA GTTGAGGTCA-3′; human *TIMP1*, forward, 5′-CATTGCTGGA AAACTGCAGGA-3′, and reverse, 5′-TCCACAAGCAATGAGT GCCA-3′; human *GAPDH*, forward, 5′-TGCACCACCAACTGCT TAG-3′, and reverse, 5′-GTTCAGCTCAGGGATGACC-3′.

Western Blot Analysis

Total protein was isolated using 1% Nonidet P-40 (NP-40). Equal amounts of protein were separated by SDS-PAGE and then transferred to a nitrocellulose membrane. The membranes were incubated with primary antibodies against mouse TIMP-1, EPR16616 (Abcam, Cambridge, UK), human TIMP-1 (Cell Signaling Technology, Danvers, MA, USA), mouse collagen type I (GeneTex, Irvine, CA, USA), mouse collagen type III (Abcam), human collagen type I (Abcam), human collagen type III, FH-7A (Abcam), or β-actin (Abcam), followed by horseradish peroxidase-conjugated anti-rabbit immunoglobulin G (IgG) (Cell Signaling Technology) or anti-mouse IgG (Cayman Chemical, Ann Arbor, MI, USA). The membranes were developed by using SuperSignal chemiluminescent substrates (Thermo Fisher Scientific). Quantification was performed using ImageJ.

Fluorescence Immunostaining for TIMP-1

Murine HS and human keloid tissues were fixed and embedded in paraffin. For murine tissues, 4-μm-thick sections were first blocked with 10% donkey serum (Sigma-Aldrich, St. Louis, MO, USA) and then incubated with a polyclonal antibody against TIMP-1 (R&D Systems), washed, and incubated with secondary antibody (Alexa Fluor 647 anti-goat IgG; Thermo Fisher Scientific). For the human tissues, 4-μm-thick sections were first blocked with 10% goat serum (Vector Laboratories, Burlingame, CA, USA) and then incubated with a monoclonal antibody against TIMP-1 (Abcam), washed, and incubated with secondary antibody (Alexa Fluor 488 anti-rabbit IgG; Abcam). Finally, the sections were mounted in medium containing 4′,6-diamidino-2-phenylindole (Vectashield with DAPI; Vector Laboratories) and observed using an Olympus fluorescence microscope (Olympus).

Gross HS Area Analysis

Images of HSs were obtained on day 14. The digital images were analyzed using GIMP 2.8. The pixel counts of the scar area were normalized to the pixel counts for the same scale.

Histological Analysis

On day 14, HS-model mice were bled and euthanized by isoflurane. The scars were resected, embedded in paraffin, and sectioned. The cross-sections were then subjected to H&E, Masson's trichrome, and picrosirius red staining, as described previously.[21] Images of sections were obtained under optical and polarized light using a microscope (Olympus). The cross-sectional area of the scars was determined using GIMP 2.8. The scar elevation index, the percentage of area of collagen, and the polarized integrated density in the scars were determined by using ImageJ as described previously.[25,50]

Microarray Analyses

The transcriptomes of the paired sCA-siCON- and sCA-siTIMP1-transfected NIH 3T3 cells were analyzed using an Agilent Technologies-based microarray platform with 8 × 60K probes. Total RNA from cells was translated into cRNA and labeled with Cy3 using the Agilent Quick Amp labeling kit (Agilent). The labeled cRNA was then purified using an RNeasy mini kit (QIAGEN). An Agilent ND-1000 was used to determine the concentration and specific activity of the labeled cRNA. Labeled cRNA from the paired control and treated samples was hybridized to the SurePrint G3 human gene expression 8 × 60K v3 microarray (Agilent). The signals were scanned using SureScan G4900DA (Agilent).

Statistical Analysis

Relative gene expression was calculated by the $2^{-\Delta\Delta Ct}$ method with correction for different amplification efficiencies. Multiple treatment groups were compared by the Tukey-Kramer method after one-way factorial ANOVA. Pairwise comparisons were performed by Student's t tests or Welch's t tests after F tests. To test for differences in the gross HS scar area, a non-parametric Wilcoxon signed-rank test was performed. Values of $p < 0.05$ were considered significant. All statistical analyses were performed using EZR (Jichi Medical University, Japan).

Data Availability

The microarray datasets have been submitted to NCBI's Gene Expression Omnibus (GEO) and are accessible through GEO: GSE128124.

SUPPLEMENTAL INFORMATION

Supplemental Information can be found online at https://doi.org/10.1016/j.omtn.2020.08.005.

AUTHOR CONTRIBUTIONS

M.A. designed the experiments and wrote the manuscript. M.A., N.M.M., and Y.O. performed the experiments and analyzed the data. T.D., H.K., and S.A. contributed to the experiments. R.O. supervised the experiments. H.Y. and K.T. contributed to the methodology. K.T. supervised the experiments and performed a critical review.

CONFLICTS OF INTEREST

The authors declare no competing interests.

ACKNOWLEDGMENTS

We thank Drs. Chisato Iwabuchi, Wataru Nakajima, and Nobuyuki Tanaka for valuable support. This work was supported by grants JP16K20371 and JP18K17005 from the Japan Society for the Promotion of Science (JSPS).

REFERENCES

1. Jumper, N., Paus, R., and Bayat, A. (2015). Functional histopathology of keloid disease. Histol. Histopathol. *30*, 1033–1057.
2. Ehrlich, H.P., Desmoulière, A., Diegelmann, R.F., Cohen, I.K., Compton, C.C., Garner, W.L., Kapanci, Y., and Gabbiani, G. (1994). Morphological and immunochemical differences between keloid and hypertrophic scar. Am. J. Pathol. *145*, 105–113.
3. Matsumoto, N.M., Peng, W.X., Aoki, M., Akaishi, S., Ohashi, R., Ogawa, R., and Naito, Z. (2017). Histological analysis of hyalinised keloidal collagen formation in earlobe keloids over time: collagen hyalinisation starts in the perivascular area. Int. Wound J. *14*, 1088–1093.
4. Lee, J.Y., Yang, C.C., Chao, S.C., and Wong, T.W. (2004). Histopathological differential diagnosis of keloid and hypertrophic scar. Am. J. Dermatopathol. *26*, 379–384.
5. Ogawa, R., Okai, K., Tokumura, F., Mori, K., Ohmori, Y., Huang, C., Hyakusoku, H., and Akaishi, S. (2012). The relationship between skin stretching/contraction and pathologic scarring: the important role of mechanical forces in keloid generation. Wound Repair Regen. *20*, 149–157.
6. Nakashima, M., Chung, S., Takahashi, A., Kamatani, N., Kawaguchi, T., Tsunoda, T., Hosono, N., Kubo, M., Nakamura, Y., and Zembutsu, H. (2010). A genome-wide association study identifies four susceptibility loci for keloid in the Japanese population. Nat. Genet. *42*, 768–771.
7. Andrews, J.P., Marttala, J., Macarak, E., Rosenbloom, J., and Uitto, J. (2016). Keloids: the paradigm of skin fibrosis—pathomechanisms and treatment. Matrix Biol. *51*, 37–46.
8. Kant, S.B., van den Kerckhove, E., Colla, C., Tuinder, S., van der Hulst, R.R.W.J., and Piatkowski de Grzymala, A.A. (2018). A new treatment of hypertrophic and keloid scars with combined triamcinolone and verapamil: a retrospective study. Eur. J. Plast. Surg. *41*, 69–80.
9. Carroll, W., and Patel, K. (2015). Steroids and fluorouracil for keloids and hypertrophic scars. JAMA Facial Plast. Surg. *17*, 77–79.
10. Ogawa, R., Huang, C., Akaishi, S., Dohi, T., Sugimoto, A., Kuribayashi, S., Miyashita, T., and Hyakusoku, H. (2013). Analysis of surgical treatments for earlobe keloids: analysis of 174 lesions in 145 patients. Plast. Reconstr. Surg. *132*, 818e–825e.
11. LaRanger, R., Karimpour-Fard, A., Costa, C., Mathes, D., Wright, W.E., and Chong, T. (2019). Analysis of keloid response to 5-fluorouracil treatment and long-term prevention of keloid recurrence. Plast. Reconstr. Surg. *143*, 490–494.
12. Al-Mohamady, Ael.-S., Ibrahim, S.M.A., and Muhammad, M.M. (2016). Pulsed dye laser versus long-pulsed Nd:YAG laser in the treatment of hypertrophic scars and keloid: A comparative randomized split-scar trial. J. Cosmet. Laser Ther. *18*, 208–212.
13. Gamil, H.D., Khattab, F.M., El Fawal, M.M., and Eldeeb, S.E. (2020). Comparison of intralesional triamcinolone acetonide, botulinum toxin type A, and their combination for the treatment of keloid lesions. J. Dermatolog. Treat. *31*, 535–544.
14. Imaizumi, R., Akasaka, Y., Inomata, N., Okada, E., Ito, K., Ishikawa, Y., and Maruyama, Y. (2009). Promoted activation of matrix metalloproteinase (MMP)-2 in keloid fibroblasts and increased expression of MMP-2 in collagen bundle regions: implications for mechanisms of keloid progression. Histopathology *54*, 722–730.
15. Ulrich, D., Ulrich, F., Unglaub, F., Piatkowski, A., and Pallua, N. (2010). Matrix metalloproteinases and tissue inhibitors of metalloproteinases in patients with different types of scars and keloids. J. Plast. Reconstr. Aesthet. Surg. *63*, 1015–1021.
16. Aoki, M., Miyake, K., Ogawa, R., Dohi, T., Akaishi, S., Hyakusoku, H., and Shimada, T. (2014). siRNA knockdown of tissue inhibitor of metalloproteinase-1 in keloid fibroblasts leads to degradation of collagen type I. J. Invest. Dermatol. *134*, 818–826.
17. Dohi, T., Miyake, K., Aoki, M., Ogawa, R., Akaishi, S., Shimada, T., Okada, T., and Hyakusoku, H. (2015). Tissue inhibitor of metalloproteinase-2 suppresses collagen synthesis in cultured keloid fibroblasts. Plast. Reconstr. Surg. Glob. Open *3*, e520.
18. Wu, X., Yamamoto, H., Nakanishi, H., Yamamoto, Y., Inoue, A., Tei, M., Hirose, H., Uemura, M., Nishimura, J., Hata, T., et al. (2015). Innovative delivery of siRNA to solid tumors by super carbonate apatite. PLoS ONE *10*, e0116022.
19. Tamai, K., Mizushima, T., Wu, X., Inoue, A., Ota, M., Yokoyama, Y., Miyoshi, N., Haraguchi, N., Takahashi, H., Nishimura, J., et al. (2018). Photodynamic therapy using indocyanine green loaded on super carbonate apatite as minimally invasive cancer treatment. Mol. Cancer Ther. *17*, 1613–1622.
20. Chowdhury, E.H., and Akaike, T. (2007). High performance DNA nano-carriers of carbonate apatite: multiple factors in regulation of particle synthesis and transfection efficiency. Int. J. Nanomedicine *2*, 101–106.
21. Aarabi, S., Bhatt, K.A., Shi, Y., Paterno, J., Chang, E.I., Loh, S.A., Holmes, J.W., Longaker, M.T., Yee, H., and Gurtner, G.C. (2007). Mechanical load initiates hypertrophic scar formation through decreased cellular apoptosis. FASEB J. *21*, 3250–3261.
22. Wong, V.W., Rustad, K.C., Akaishi, S., Sorkin, M., Glotzbach, J.P., Januszyk, M., Nelson, E.R., Levi, K., Paterno, J., Vial, I.N., et al. (2011). Focal adhesion kinase links mechanical force to skin fibrosis via inflammatory signaling. Nat. Med. *18*, 148–152.
23. Yasuoka, H., Larregina, A.T., Yamaguchi, Y., and Feghali-Bostwick, C.A. (2008). Human skin culture as an ex vivo model for assessing the fibrotic effects of insulin-like growth factor binding proteins. Open Rheumatol. J. *2*, 17–22.
24. Ibaraki, H., Kanazawa, T., Takashima, Y., Okada, H., and Seta, Y. (2016). Development of an innovative intradermal siRNA delivery system using a combination of a functional stearylated cytoplasm-responsive peptide and a tight junction-opening peptide. Molecules *21*, 1279.
25. Ye, X., Pang, Z., and Zhu, N. (2019). Dihydromyricetin attenuates hypertrophic scar formation by targeting activin receptor-like kinase 5. Eur. J. Pharmacol. *852*, 58–67.
26. Lebeko, M., Khumalo, N.P., and Bayat, A. (2019). Multi-dimensional models for functional testing of keloid scars: in silico, in vitro, organoid, organotypic, ex vivo organ culture, and in vivo models. Wound Repair Regen. *27*, 298–308.
27. Lee, W.J., Lee, J.H., Ahn, H.M., Song, S.Y., Kim, Y.O., Lew, D.H., and Yun, C.O. (2015). Heat shock protein 90 inhibitor decreases collagen synthesis of keloid fibroblasts and attenuates the extracellular matrix on the keloid spheroid model. Plast. Reconstr. Surg. *136*, 328e–337e.
28. Das, S., Ghosal, S., Chakrabarti, J., and Kozak, K. (2013). SeedSeq: off-target transcriptome database. BioMed Res. Int. *2013*, 905429.
29. Rosa, J., Suzuki, I., Kravicz, M., Caron, A., Pupo, A.V., Praça, F.G., and Bentley, M.V.L.B. (2018). Current non-viral siRNA delivery systems as a promising treatment of skin diseases. Curr. Pharm. Des. *24*, 2644–2663.
30. Chernikov, I.V., Vlassov, V.V., and Chernolovskaya, E.L. (2019). Current development of siRNA bioconjugates: from research to the clinic. Front. Pharmacol. *10*, 444.
31. Aldawsari, M., Chougule, M.B., and Babu, R.J. (2015). Progress in topical siRNA delivery approaches for skin disorders. Curr. Pharm. Des. *21*, 4594–4605.
32. Chen, M., Zakrewsky, M., Gupta, V., Anselmo, A.C., Slee, D.H., Muraski, J.A., and Mitragotri, S. (2014). Topical delivery of siRNA into skin using SPACE-peptide carriers. J. Control. Release *179*, 33–41.

33. Kenski, D.M., Butora, G., Willingham, A.T., Cooper, A.J., Fu, W., Qi, N., Soriano, F., Davies, I.W., and Flanagan, W.M. (2012). siRNA-optimized modifications for enhanced in vivo activity. Mol. Ther. Nucleic Acids *1*, e5.

34. Chan, D.P.Y., Deleavey, G.F., Owen, S.C., Damha, M.J., and Shoichet, M.S. (2013). Click conjugated polymeric immuno-nanoparticles for targeted siRNA and antisense oligonucleotide delivery. Biomaterials *34*, 8408–8415.

35. Fernando, O., Tagalakis, A.D., Awwad, S., Brocchini, S., Khaw, P.T., Hart, S.L., and Yu-Wai-Man, C. (2018). Development of targeted siRNA nanocomplexes to prevent fibrosis in experimental glaucoma filtration surgery. Mol. Ther. *26*, 2812–2822.

36. Rabbani, P.S., Zhou, A., Borab, Z.M., Frezzo, J.A., Srivastava, N., More, H.T., Rifkin, W.J., David, J.A., Berens, S.J., Chen, R., et al. (2017). Novel lipoproteoplex delivers *Keap1* siRNA based gene therapy to accelerate diabetic wound healing. Biomaterials *132*, 1–15.

37. Li, N., Luo, H.C., Yang, C., Deng, J.J., Ren, M., Xie, X.Y., Lin, D.Z., Yan, L., and Zhang, L.M. (2014). Cationic star-shaped polymer as an siRNA carrier for reducing MMP-9 expression in skin fibroblast cells and promoting wound healing in diabetic rats. Int. J. Nanomedicine *9*, 3377–3387.

38. Nemati, H., Ghahramani, M.H., Faridi-Majidi, R., Izadi, B., Bahrami, G., Madani, S.H., and Tavoosidana, G. (2017). Using siRNA-based spherical nucleic acid nanoparticle conjugates for gene regulation in psoriasis. J. Control. Release *268*, 259–268.

39. Morry, J., Ngamcherdtrakul, W., Gu, S., Goodyear, S.M., Castro, D.J., Reda, M.M., Sangvanich, T., and Yantasee, W. (2015). Dermal delivery of HSP47 siRNA with NOX4-modulating mesoporous silica-based nanoparticles for treating fibrosis. Biomaterials *66*, 41–52.

40. Aoki, M., Aoki, H., Mukhopadhyay, P., Tsuge, T., Yamamoto, H., Matsumoto, N.M., Toyohara, E., Okubo, Y., Ogawa, R., and Takabe, K. (2019). Sphingosine-1-phosphate facilitates skin wound healing by increasing angiogenesis and inflammatory cell recruitment with less scar formation. Int. J. Mol. Sci. *20*, 3381.

41. Alkan, F., Wenzel, A., Palasca, O., Kerpedjiev, P., Rudebeck, A.F., Stadler, P.F., Hofacker, I.L., and Gorodkin, J. (2017). RIsearch2: suffix array-based large-scale prediction of RNA-RNA interactions and siRNA off-targets. Nucleic Acids Res. *45*, e60.

42. Wei, J.W., Huang, K., Yang, C., and Kang, C.S. (2017). Non-coding RNAs as regulators in epigenetics (Review). Oncol. Rep. *37*, 3–9.

43. Lynch, J.J., 3rd, Van Vleet, T.R., Mittelstadt, S.W., and Blomme, E.A.G. (2017). Potential functional and pathological side effects related to off-target pharmacological activity. J. Pharmacol. Toxicol. Methods *87*, 108–126.

44. Ogawa, R. (2017). Keloid and hypertrophic scars are the result of chronic inflammation in the reticular dermis. Int. J. Mol. Sci. *18*, 606.

45. Huang, C., Liu, L., You, Z., Du, Y., and Ogawa, R. (2019). Managing keloid scars: from radiation therapy to actual and potential drug deliveries. Int. Wound J. *16*, 852–859.

46. Shi, F., Cao, X., Hu, Z., Ma, D., Guo, D., Zhang, J., Zhang, C., Liu, P., Qu, S., Zhu, J., et al. (2017). Pleiotropic FTY720 is a specific and potent therapy for hypertrophic scars. J. Invest. Dermatol. *137*, 1552–1561.

47. Ogawa, R., Akaishi, S., Dohi, T., Kuribayashi, S., Miyashita, T., and Hyakusoku, H. (2015). Analysis of the surgical treatments of 63 keloids on the cartilaginous part of the auricle: effectiveness of the core excision method. Plast. Reconstr. Surg. *135*, 868–875.

48. Castleberry, S.A., Golberg, A., Sharkh, M., Khan, S., Aimquist, B.D., Austen, W.G., Jr., et al. (2016). Nanolayered siRNA delivery platforms for local silencing of CTGF reduce cutaneous scar contraction in third-degree burns. Biomaterials *95*, 22–34.

49. Berman, B., Maderal, A., and Raphael, B. (2017). Keloids and hypertrophic scars: pathophysiology, classification, and treatment. Dermatol. Surg. *43* (*Suppl 1*), S3–S18.

50. Chen, Y., Yu, Q., and Xu, C.-B. (2017). A convenient method for quantifying collagen fibers in atherosclerotic lesions by ImageJ software. Int. J. Clin. Exp. Med. *10*, 14904–14910.